



De novo structural variants in autism spectrum disorder disrupt distal regulatory interactions of neuronal genes

Ketrin Gjoni, Xingjie Ren, Amanda Everitt, et al.

Genome Res. published online July 8, 2026

Access the most recent version at doi:[10.1101/gr.280394.124](https://doi.org/10.1101/gr.280394.124)

P<P	Published online July 8, 2026 in advance of the print journal.
Accepted Manuscript	Peer-reviewed and accepted for publication but not copyedited or typeset; accepted manuscript is likely to differ from the final, published version.
Open Access	Freely available online through the <i>Genome Research</i> Open Access option.
Creative Commons License	This manuscript is Open Access. This article, published in <i>Genome Research</i> , is available under a Creative Commons License (Attribution-NonCommercial 4.0 International license), as described at http://creativecommons.org/licenses/by-nc/4.0/ .
Email Alerting Service	Receive free email alerts when new articles cite this article - sign up in the box at the top right corner of the article or click here .

Comprehensive immune receptor profiling.
Discover the **DriverMap™ AIR Assay** difference.

LEARN
MORE



To subscribe to *Genome Research* go to:
<https://genome.cshlp.org/subscriptions>

Published by Cold Spring Harbor Laboratory Press

1 **De novo structural variants in autism spectrum disorder disrupt distal regulatory interactions of**
2 **neuronal genes.**

3 Ketrin Gjoni^{1,2}, Xingjie Ren³, Amanda Everitt^{1,2}, Yin Shen^{3,4,5}, Katherine S. Pollard^{1,2,6,7}

4

5 ¹Gladstone Institute of Data Science and Biotechnology, San Francisco, CA 94158

6 ²Department of Epidemiology & Biostatistics, University of California, San Francisco, CA 94158

7 ³Institute for Human Genetics, University of California, San Francisco, San Francisco, CA 94143

8 ⁴Department of Neurology, University of California, San Francisco, San Francisco, CA 94143

9 ⁵Weill Institute for Neurosciences, University of California, San Francisco, San Francisco, CA 94158

10 ⁶Bakar Computational Health Sciences Institute, University of California, San Francisco, CA 94143

11 ⁷Chan Zuckerberg Biohub, San Francisco, CA 94158

12

13 *Katherine S. Pollard

14 Gladstone Institutes

15 1650 Owens Street

16 San Francisco, CA

17 94158

18 USA

19 415-734-2711

20 **Email:** katherine.pollard@gladstone.ucsf.edu

21

22 Variants disrupt neuronal regulatory interactions

23 Abstract

24

25 Three-dimensional genome organization plays a critical role in gene regulation, and disruptions can lead
26 to developmental disorders by altering the contact between genes and their distal regulatory elements.
27 Structural variants (SVs) can disturb local genome organization, such as the merging of topologically
28 associating domains upon boundary deletion. Testing large numbers of SVs experimentally for their
29 effects on chromatin structure and gene expression is time- and cost- prohibitive. To address this, we
30 propose a computational approach to predict SV impacts on genome folding, which can help prioritize
31 causal hypotheses for functional testing. We develop a weighted scoring method that measures chromatin
32 contact changes specifically affecting regions of interest, such as regulatory elements or promoters, and
33 implement it in the SuPreMo-Akita software (Gjoni and Pollard 2024). With this tool, we rank hundreds
34 of de novo SVs (dnSVs) from autism spectrum disorder (ASD) individuals and their unaffected siblings
35 based on predicted disruptions to nearby neuronal regulatory interactions. This reveals that putative *cis*-
36 regulatory element interactions (CREints) are more disrupted by dnSVs from ASD probands versus
37 unaffected siblings. We prioritize candidate variants that disrupt ASD CREints and validate our top-
38 ranked locus using isogenic excitatory neurons with and without the dnSV, confirming accurate
39 predictions of disrupted chromatin contacts. This study suggests that disrupted genome folding is a
40 potential genetic mechanism in a subset of ASD cases and provides a general strategy for prioritizing
41 variants predicted to disrupt regulatory interactions across tissues.

42 **Introduction**

43

44 The human genome is folded into organized and hierarchical three-dimensional (3D) structures that span
45 DNA loops, which bring two loci together, topologically associating domains (TADs), which insulate
46 contact from surrounding regions, and compartments, which delineate regions of the genome based on
47 activity. This complex multilayered system plays a critical role in regulating gene expression, in part by
48 controlling the interactions between promoters and distal regulatory elements. Advancements in
49 chromosome conformation capture technologies, such as HiC(van Berkum et al. 2010) and
50 MicroC(Krietenstein et al. 2020), have enabled the understanding of the interplay between the 3D genome
51 and cellular function. Disruption of chromatin structures can lead to pathogenic re-wiring of regulatory
52 interactions of disease-associated genes(Krumm and Duan 2019). For example, the fusion of two TADs
53 can cause enhancer hijacking, whereby a gene in one TAD becomes regulated by a new enhancer and is
54 differentially expressed. Furthermore, chromatin organization of neuronal cells plays a critical role in
55 brain development and the onset of neurological disorders(Zagirova et al. 2024), and recent work has
56 shown that de novo promoter variants within TADs containing ASD genes are significantly associated
57 with autism risk(Nakamura et al. 2024).

58

59 Structural variants (SVs)—a class of mutations encompassing large deletions, insertions, duplications,
60 inversions, chromosomal rearrangements or combinations of these—have the potential to disrupt 3D
61 genome structures and cause disease(Sikic 2023; Weischenfeldt and Ibrahim 2023). Germline SVs have
62 been shown to cause gene misregulation and contribute to cancer and developmental diseases such as
63 limb malformations(Symmons et al. 2016), X-Chromosome inactivation(van Bommel et al. 2019), limb
64 morphogenesis(Kragesteen et al. 2018), congenital malformations(Kraft et al. 2019), branchiooculofacial
65 syndrome(Laugsch et al. 2019), Fragile X syndrome(Sun et al. 2018), and Cooks syndrome(Kurth et al.
66 2009). This evidence highlights the phenotypic consequences of disrupted genome structure in

67 development and suggests the importance of further investigating SVs that alter genome folding as a
68 potential causal mechanism in genetic disorders with poorly understood causes.

69
70 Since disrupted genome structure that leads to misexpression of critical genes has been characterized in
71 many developmental disorders, we hypothesize that this mechanism is present in autism spectrum
72 disorder (ASD). ASD is a class of neurodevelopmental conditions with complex causes that span
73 environmental risk factors and genetics(Chaste and Leboyer 2012), with approximately equal
74 contribution(Huguet et al. 2016). While the heritability is estimated to be 40-80%(Rylaarsdam and
75 Guemez-Gamboa 2019), the genetic mechanisms are largely not understood with 80% of cases remaining
76 without a genetic cause(Geschwind 2011). Most studies that investigate the genetic causes of ASD focus
77 on identifying common risk variants, mostly single nucleotide polymorphisms (SNPs)(Grove et al. 2019)
78 or small insertions or deletions (indels). However, small sample sizes do not have enough statistical
79 power to identify rare or low-risk variants, which can only be characterized if they fall on candidate risk
80 genes(More et al. 2023; Iossifov et al. 2014) but otherwise have largely unknown effects. Evaluating the
81 effect of rare variants is important because de novo mutations have been strongly implicated in
82 ASD(Iossifov et al. 2014; Short et al. 2018; An et al. 2018; Satterstrom et al. 2020), and are estimated to
83 contribute to about 10% of ASD cases(Huguet et al. 2016). Furthermore, de novo variants are more likely
84 to be causal in simplex families, in which only one offspring has been diagnosed with ASD. Some studies
85 evaluated de novo variants using machine learning (ML) models to predict their effects on gene
86 expression and found proband variants to be more damaging than those of siblings(Zhou et al. 2019;
87 Kelley 2020). As this work did not include structural variants, there is a need for further evaluation of de
88 novo structural variants (dnSVs) in ASD.

89
90 To evaluate ASD variants with unknown contribution to the disorder, we sought to predict if they disrupt
91 chromatin organization nearby neuronal developmental genes. Functionally characterizing variants
92 requires individually evaluating their effect on gene expression and the accompanying mechanism, which

93 is experimentally infeasible at scale due to time and cost limitations. To overcome this, ML models can
94 be used with *in silico* mutagenesis (ISM) to predict variant deleteriousness at scale and prioritize
95 candidate variants for experimental evaluation. One such model is Akita, a convolutional neural network
96 (CNN) that predicts high resolution contact frequency maps for multiple cell types from genomic
97 sequence alone with very high accuracy (genome-wide test set average MSE=0.14, Spearman's
98 $R=0.56$)(Fudenberg et al. 2020). By making and comparing predictions for sequences with and without a
99 mutation, ISM with Akita enables researchers to score its effect on 3D genome structure. For example,
100 Akita accurately predicted how sequence variants that arose during hominid evolution altered genome
101 folding in human versus chimpanzee neural progenitor cells(Keough et al. 2023). We previously
102 developed SuPreMo-Akita(Gjoni and Pollard 2024), a computational pipeline that streamlines ISM with
103 Akita allowing us to test massive numbers of rare and complex variants for their effects on genome
104 structure, prioritizing variants and generating testable hypotheses about their effects on disease-relevant
105 genes.

106

107 However, SuPreMo-Akita does not specifically identify changes in genome folding that affect gene
108 regulatory interactions. To address this limitation, we combined a weighted scoring SuPreMo-Akita
109 framework, leveraging excitatory neuron (ExN) PLAC-seq data(Song et al. 2020) to evaluate the effects
110 of dnSVs present in ASD individuals(Belyeu et al. 2021) versus unaffected sibling controls, with
111 CRISPR-engineered induced pluripotent stem cell (iPSC)-derived ExNs to validate model predictions in
112 one locus. The results provide a proof-of-concept for prioritizing variants of unknown significance for
113 their effects on chromatin interactions and generating testable hypotheses.

114 **Results**

115

116 **Large ASD dnSVs disrupt genome structure.**

117 In this study, we used dnSVs from simplex families in the Simons Foundation Autism Research Initiative
118 (SFARI) Simons Simplex Collection (SSC) cohort (Belyeu et al. 2021; Fischbach and Lord 2010).

119 Variants from ASD probands (n=521) and their unaffected siblings (n=348) were previously called from
120 short-read whole genome sequencing (Belyeu et al. 2021). We scored these variants for their predicted
121 effects on 3D genomic contacts in the surrounding region using previously published SuPreMo-

122 Akita (Gjoni and Pollard 2024) (**Fig. 1A, Methods, Supplemental Table S1**). As a part of this pipeline,
123 contact frequency maps that correspond to the reference and alternate allele and the surrounding region
124 are compared using Spearman's correlation (hereafter referred to as correlation). The resulting score (1 -
125 correlation) is a measure of how disruptive each variant is to genomic contacts in the surrounding ~1 Mb
126 region. If the variant has no effect, the correlation is close to one and the score is approximately zero.

127 Disruption scores were generated for a subset of dnSVs that are compatible with SuPreMo-Akita based on
128 their length, type, and region (**Methods**). Across the 598 scored variants, the mean disruption score was
129 higher for proband dnSVs than for sibling dnSVs (**Fig. 1B, S1B**). While statistically significant, the effect
130 size is small (Cohen's $d = 0.18$), and the difference is driven by a subset of highly disruptive variants
131 rather than a global shift. The disruption score distributions for both groups are left skewed with most
132 variants resulting in low disruption to genome folding, consistent with other studies generating ISM
133 disruption scores with Akita (Gunsalus et al. 2023a, 2023b). But the highest scoring variants (1 -
134 correlation > 0.2) include more proband than sibling dnSVs (14% vs. 7% of dnSVs from each group),
135 suggesting that the difference in means is driven by high scoring variants. Overall, high scoring variants
136 are found in 15% of probands and only 8% of siblings.

137

138 In order to understand factors that contribute to high scoring proband dnSVs, we looked at how scores
139 relate to variant length, its type, and functional features that it overlaps. We find that dnSV length is
140 positively correlated with disruption scores, with longer variants causing bigger changes to genomic
141 contacts (**Fig. 1C**). We therefore grouped variants by their length quantiles, to ensure the differences
142 between proband and sibling dnSVs are not solely due to length differences. When controlling for dnSV
143 length, we find that the difference between proband and sibling dnSVs is driven by larger variants from
144 the fourth length quantile (**Fig. 1D**). This further supports the idea that large variants are driving these
145 differences, whereas smaller variants are similarly damaging in probands versus siblings. Next, we
146 evaluated how disruption scores compare across variant types and found significant differences, namely
147 that duplications are the most disruptive and inversions the least (**Fig. 1E**). This trend could be partially
148 explained by dnSV length since duplications are also the largest variants in this dataset, while inversions
149 are the smallest (**Fig. 1F**). Nonetheless, these trends do not contribute to the difference in scores between
150 proband and sibling dnSVs, because the two groups have similar distributions of variant types
151 (**Supplemental Fig. S1C-D**).

152
153 We then evaluated whether genome structure disruption scores are related to variant overlap with CTCF
154 binding sites, epigenetic marks, disruption scores from other sequence-based models, or to the polygenic
155 risk scores of the individuals carrying them. We categorized dnSVs by length quantiles, and found that
156 large high scoring dnSVs have stronger CTCF and H3K27ac ChIP-seq signal than low scoring large
157 dnSVs, while there is no difference in signal for other epigenomic marks such as ATAC-seq and
158 H3K27me3 and H3K4me1 ChIP-seq (**Supplemental Fig. S1E**). Given that CTCF contributes to genome
159 structure through cohesin-mediated loop extrusion, we expected variants that disrupt CTCF binding to
160 result in larger changes to genome folding. While we see this pattern across both proband and sibling
161 dnSVs, the association is stronger in probands (**Supplemental Fig. S1F**). Interestingly, long dnSVs are
162 significantly more disruptive when overlapping CTCF in probands but not in siblings (**Fig. 1G**). This
163 suggests that proband dnSVs disrupt CTCF binding sites that are more important for genome folding and

164 result in more consequential changes when disrupted compared to sibling dnSVs. Next, we compared
165 Akita disruption scores to those from another sequence-based model, DeepSEA, which predicts various
166 chromatin profiles excluding genome structure. While there were a few variants that were ranked highly
167 from both methods—for example a variant ranked through DeepSEA’s H3K27me3 score in H1-hESCs—
168 overall Akita disruption scores were poorly correlated with DeepSEA scores (less than 0.15 across all
169 tracks), underscoring that Akita captures complementary information (**Supplemental Fig. S1G**).

170

171 Lastly, we checked if an individual’s ASD polygenic risk score(Weiner et al. 2017) is associated with
172 their dnSV disruption score or dnSV length, to find that this is not the case neither in probands nor
173 siblings (**Supplemental Fig. S1H-I**). Taken together, these results show that proband dnSVs are slightly
174 but significantly more damaging to chromatin organization than the unaffected sibling dnSVs—at least
175 partially due to disruption of CTCF binding sites—suggesting that disrupted genome folding might play a
176 role in the genetic etiology of ASD.

177

178 **ASD dnSVs disrupt neighboring neuronal regulatory element contacts**

179 To focus our scoring approach on variants where the altered chromatin contacts affect regulatory elements
180 and their target genes, we defined putative *cis*-regulatory element interactions (CREints) as chromatin
181 interactions that are within the ~1 Mb prediction window, and correspond to the promoter of an expressed
182 gene (**Supplemental Fig. S2A, Methods**). To apply this approach to ASD, we used H3K4me3 PLAC-seq
183 and RNA-seq data from primary ExNs(Song et al. 2020)—the cell type most implicated in the
184 disorder(Willsey et al. 2022). We observed that proband but not sibling noncoding dnSVs are enriched
185 near CREints (**Supplemental Fig. S2B**). This suggests that while these variants do not directly impact
186 any coding sequences, they have potential to alter regulatory interactions of genes expressed in ExNs.

187

188 Motivated by this observation, we sought to specifically evaluate the effect of dnSVs on gene regulation
189 by generating scores that only reflect disrupted interactions at CREint anchors (putative promoter and

190 regulatory element). We developed a weighted scoring method which is flexible to various annotation
191 types and can be tuned to emphasize regions of interest (ROIs) while still considering changes within the
192 locus (**Fig. 2A, Methods**). Instead of comparing the maps as a whole, we calculated disruption scores by
193 averaging the disruption at each bin in the prediction window (**Fig. 2A**: disruption track in purple). This
194 allows for calculating the weighted average by multiplying the disruption track by an ROI weight track
195 before taking the mean (**Fig. 2A**: weight track in orange). The weight track upscales disruptions at bins
196 corresponding to ROIs by a user-specified amount. Weighted disruption scores are lower than unweighted
197 scores when there is less disruption at ROI bins versus the rest of the map (**Supplemental Fig. S2Ci**),
198 greater than unweighted scores when there is more disruption at ROI bins (**Supplemental Fig. S2Cii**),
199 and similar to unweighted scores when ROI and non-ROI bins have similar disruption values
200 (**Supplemental Fig. S2Ciii**).

201
202 To easily and scalably apply weighted scoring to the ASD dnSV dataset, and to make it accessible for
203 others working with models beyond Akita, we incorporated the method into the SuPreMo pipeline. In
204 sum, we added inputs for: ROIs and the scaling factor, the Akita-prediction cell type, and the extent to
205 shift the prediction window for each variant to include ROIs. To input ROIs and scaling factors,
206 arguments '--roi' and '--scale' can be used to provide regions to upweight and the amount to upweight by,
207 respectively. These ROIs can be PLAC-seq paired regions, custom regions, or TSSs for example (**Fig 2A,**
208 **Methods**). To include neighboring ROIs in the prediction window, the '--shifts' parameter can be used to
209 specify the up- or down- stream shifting amount for each variant. This shifting feature also makes
210 SuPreMo compatible with models, like ExPecto(Zhou et al. 2018), that require centering a TSS instead of
211 the variant. The adapted SuPreMo pipeline with all these modifications was released as version 2 (V2) on
212 GitHub (**Methods**).

213
214 With this tool in hand, we turned back to evaluating dnSVs likely to change chromatin contacts that affect
215 neuronal CREints in ASD probands and unaffected siblings. We focused on the 319 dnSVs that are near

216 at least one CREint. Our original scores did not show significant differences between probands and
217 siblings for this subset of dnSVs (Mann-Whitney U test p -value 0.36). We then paired each dnSV with all
218 the nearby CREints and used custom shifting to make predictions centering each dnSV and CREint pair
219 (**Methods**). We calculated unweighted and weighted disruption scores for each pair and kept the highest
220 score for each dnSV. We used all of the CREints in the window for weighting, but found that using only
221 the paired CREint for each window did not change the trends we observed. While we see a significant
222 difference between proband and sibling dnSV unweighted scores (**Fig. 2Bi**, p -value = 0.014), weighted
223 scores enhance this difference both when up-weighting CREints by 10-fold (**Fig. 2Bii**, p -value = 0.006)
224 and when only scoring bins at CREint anchors (**Fig. 2Biii**, p -value = 0.008). Additionally, there are more
225 proband dnSVs with higher weighted versus unweighted scores (50% of dnSVs) compared to siblings
226 (36%) (**Supplemental Fig. S2D-E**). This data suggests that proband dnSVs are more disruptive at
227 CREints and are therefore more likely to have a functional impact in ExNs. For the majority of variants, if
228 scores at CREints were higher than unweighted scores, CREint scores were the highest, further supporting
229 that changes are concentrated at CREint anchors (**Supplemental Fig. S2E**). In summary, we found that
230 proband dnSVs are more disruptive to neuronal promoters and their distal regulatory elements as
231 compared to sibling dnSVs and that predicted changes in chromatin contacts in disrupted loci are
232 concentrated on the regulatory interactions. These results further support our hypothesis that proband
233 dnSVs contribute to ASD partially through 3D genome folding disruption.

234

235 **Prioritizing candidate dnSVs likely to affect ASD genes**

236 Our SuPreMo-Akita weighted disruption scores produced a testable hypothesis for each dnSV about what
237 regulatory interactions it may alter in neurons. Genome editing and induced pluripotent stem cells provide
238 experimental tools for investigating these hypotheses. Since generating stable, isogenic cell lines is
239 currently relatively low throughput, we sought to prioritize a small number of dnSVs with compelling
240 evidence in support of functional characterization. To do so, we compiled information about the variant,
241 the prediction, and the proband, organizing these data into 7 required and 5 optional criteria. These

242 criteria prioritize disruptive dnSVs near—but not overlapping—ASD genes, have robust Akita predictions,
243 and occur in probands without a high risk variant elsewhere in their genome (**Methods, Supplemental**
244 **Fig. S3A**). Most dnSVs meet 4-5 of the required criteria, and typically proband dnSVs meet more criteria
245 than sibling dnSVs (**Supplemental Fig. S3B**). Nine dnSVs passed all 7 required criteria and were
246 evaluated both on the 5 optional criteria and on qualitative characteristics, such as visually inspecting how
247 strong the changes are, where they fall with respect to ASD genes, and how PLAC-seq loops support the
248 prediction (**Methods**).

249

250 With this selection process, we identified three proband dnSVs that have the potential to contribute to
251 ASD by misregulating associated genes through 3D genome folding disruption (**Supplemental Fig.**
252 **S3C**). First, a 160 base pair (bp) deletion in Chromosome 17 (**Supplemental Fig. S3Ci**) lowers contact
253 frequency at and near *RAI1* (arrows), a high confidence and syndromic SFARI gene (Banerjee-Basu and
254 Packer 2010). *RAI1* is a transcriptional regulator of the circadian clock involved in embryonic
255 development and neural differentiation (Huang et al. 2016). In another proband, a 2 Mb duplication
256 encompasses *RAI1* further supporting its association with ASD. This deletion overlaps a *MYO15A* exon,
257 but the gene is lowly expressed in ExN and not relevant in ASD. Second, a 1.6 kb deletion in
258 Chromosome 9 (**Supplemental Fig. S3Cii**) results in slightly decreased contacts of *STXBPI* (arrows), a
259 high confidence SFARI candidate involved in 49 ASD cases that plays a role in neurotransmitter
260 release (Banerjee-Basu and Packer 2010). Of note, this variant was found in a proband that also has a
261 missense mutation in an exon of *SNX14*, a syndromic SFARI gene, which might contribute to their
262 genetic cause of ASD. This is an intronic deletion in *NIBAN2* and overlaps two ExN H3K27ac peaks.
263 Lastly, a 23 kb deletion in Chromosome 10 (**Supplemental Fig. S3Ciii**) lies in a locus rich with
264 neurodevelopmental genes, including *PPP3CB*, which is downregulated in two in vivo ASD models (Xia
265 et al. 2024; Liu et al. 2023), *CAMK2G*, which is linked to neurodevelopmental disorders and associated
266 with ASD, and *P4HAI*, which was found to be associated with ASD in a de novo risk score analysis (An
267 et al. 2018). The deletion overlaps 8 exons of *USP54*, which is not involved in ASD or neurodevelopment

268 and has a very low probability of loss of function ($pLI = 0$) suggesting this heterozygous deletion may not
269 affect USP54 protein function. While the deletion does not overlap any ExN regulatory marks, it removes
270 a CTCF binding site suggesting that the mechanism behind the changed contact maps includes the loss of
271 an insulating boundary. Indeed, disruption scores from tiled 1 bp deletions across the dnSV recapitulate
272 the CTCF motif (**Supplemental Fig. S5A**), also highlighting Akita's ability to capture the grammar of
273 genomic determinants of 3D genome folding. Together, these features made this Chromosome 10 variant
274 the strongest candidate of the five and prompted us to experimentally test the predictions.

275

276 **In vitro variant model validates predictions and suggests transcriptomic impact**

277 Since regulatory interactions are likely to vary across cell types, neuronal chromatin folding patterns are
278 different from non-neuronal cells (Zagirova et al. 2024), and ASD largely affects ExNs, we characterized
279 the Chromosome 10 proband dnSV in WTC11 i^3N iPSC-induced ExNs (38). Using a CRISPR-Cas9-
280 mediated deletion in the WTC11 i^3N iPSC line (Wang et al. 2017), we generated two clonal cell lines with
281 a homozygous deletion similar to the variant ("full deletion"; **Supplemental Fig. S4A, Methods,**
282 **Supplemental Table S2**), allowing us to isolate the effects of the deletion on genome folding without
283 being influenced by an unedited copy. In contrast to the variant in the proband, which affects exons 11-
284 18, is in frame, and should result in a partial mRNA expression of 14 exons of *USP54*, the engineered
285 clones harbor a deletion of part of exon 13 and exons 14-18, and result in an early stop codon with in
286 frame transcription resuming after the deletion, including exons 19-22 (**Supplemental Fig. S4B-C**).
287 USP54 is involved in ubiquitin-proteasome-dependent proteolysis and is expressed in primary ExNs
288 (TPM = 16) (Song et al. 2020). We differentiated two unedited (WT) and the two isogenic full deletion
289 clones into ExNs and performed Hi-C to evaluate chromatin interactions (**Methods**). The contact
290 frequency map from WT ExNs matched the Akita prediction from the reference human genome fairly
291 well (Spearman's correlation = 0.61), and the observed effect of the deletion on the map was highly
292 similar to our prediction for the proband variant (**Fig. 3**). Namely, the overall pattern of the strengthened
293 contact (purple) between the TAD boundaries, the decreased contact (green) of the upstream boundary

294 with inter-TAD regions (left arrow), and increased contact of the downstream boundary with inter-TAD
295 regions (right arrow), are consistent between the prediction and experimental Hi-C data, despite a few
296 quantitative differences where the experiment indicates larger effects. To test whether the predicted
297 changes were due to the deleted CTCF binding site specifically, we generated two additional clonal cell
298 lines in which only the CTCF ChIP-seq peak was deleted (“CTCF deletion”; **Supplemental Fig. S4A-C**).
299 Both reference and CTCF deletion contact frequency maps matched Akita predictions, resulting in a
300 similar, but less strong, effect as the full deletion (**Supplemental Fig. S5B-C**). The more striking changes
301 caused by the full deletion suggest that while the CTCF binding site plays a role in chromatin interactions
302 in this locus, additional sequences within the full ASD dnSV likely also contribute.

303

304 To evaluate the effect of the Chromosome 10 deletion on gene expression, we performed RNA-seq on
305 cell lines from all three conditions (2 WT, 2 full deletion, 2 CTCF deletion). We first evaluated the effect
306 of the deletions on *USP54* and found that its transcription continued after both deletion types
307 (**Supplemental Fig. S6A**). A principal component analysis (PCA) of the gene expression data clearly
308 separated all three editing conditions (**Supplemental Fig. S6B**). It is unclear how much of the separation
309 between the full deletion and CTCF deletion cell lines is due to the strength of the variant-caused contact
310 change or the differing effect on *USP54*. We focus our next analyses on the full deletion since it is similar
311 to the variant found in the proband and the in vitro changes are most likely to mirror its expected effect.
312 We then performed a genome-wide differential gene expression analysis and found that the full deletion
313 resulted in 1,102 differentially expressed genes (DEGs) (**Supplemental Fig. S6C and Supplemental**
314 **Table S3**). Interestingly, full deletion DEGs are enriched for GO terms involving neuron development,
315 differentiation, and function, when using all expressed genes as a background (**Supplemental Fig. S6D**
316 **and Supplemental Table S4**). They are also enriched for ASD genes (**Supplemental Fig. S6E-F**).
317 Though the damaged *USP54* transcript likely imparts some differential expression signal, we do not see
318 enrichment of genes from the Ubiquitin-Proteasome Dependent Proteolysis pathway in either deletion cell
319 line (**Supplemental Fig. S6E-F**), suggesting it is not a dominant driver. Since the deletion overlaps

320 neither PLAC-seq loops nor NPC H3K27ac and H3K4me3 ChIP-seq peaks (**Supplemental Fig. S7A**),
321 the effects do not seem to be due to direct removal of regulatory elements. To further assess coordinated
322 transcriptomic effects, we performed a weighted gene co-expression network analysis and identified 43
323 gene co-expression modules, of which four were significantly associated with the deletion cell line
324 (**Supplemental Fig. S7B**). All four modules included at least one gene that is within 5 kb of the deletion
325 (included in Fig. 3) and three of them included *DDIT4*. The turquoise module—which had the most gene
326 near the deletion—was strongly enriched for neurodevelopmental processes such as neuron differentiation,
327 axon development, and axonogenesis (**Supplemental Fig. S7C**). Overall, the transcriptomic effects of the
328 Chromosome 10 deletion cell model further support its potential to affect the function of neuronal cells.
329

330 Given these broad transcriptional changes and the lack of direct regulatory element disruption, we next
331 asked whether altered 3D genome contacts could underlie the observed misregulation. We speculate that
332 changes in genomic folding caused by the deletion may perturb long-range regulatory interactions,
333 misregulating genes near the breakpoint and triggering cascading transcriptomic effects genome-wide.
334 Interestingly, the full deletion did not affect the expression of genes within the ~1 Mb Akita prediction
335 window; however, Hi-C data allow us to evaluate potential effects beyond this narrow range. These long-
336 distance effects include regions with important neurodevelopmental genes such as *DDIT4*, which lies 1.2
337 Mb from the dnSV and may be influenced by altered chromatin contacts (**Supplemental Fig. S8A**). We
338 observe downregulation of *DDIT4* in the full deletion cell line (**Supplemental Fig. S8B**), suggesting that
339 perhaps *DDIT4* dysregulation—regardless of direction—may disrupt neuronal homeostasis and contribute to
340 ASD risk. *DDIT4* is a part of the mTOR signaling pathway, genes from which are enriched in the full
341 deletion DEGs (**Supplemental Fig. S8C**, odds ratio = 6; chi-squared p -value = $2.2e-14$), suggesting that a
342 subset of DEGs is caused by *DDIT4* downregulation. The CTCF deletion cell lines also showed similar
343 contact changes at *DDIT4* and decreased expression although both these changes are less pronounced than
344 in the full deletion (**Supplemental Fig. S8A-B**). While the role of the 3D genome folding changes caused
345 by the full deletion on gene expression is unclear, this data suggests a scenario where the variant impacts

346 DDIT4 expression by disrupting its distal regulatory contacts and in turn misregulating an array of genes
347 in its pathway. Other nearby DEGs that could have a similar effect are *SPOCK2*, which is thought to be
348 involved in neurogenesis, and *UNC5B*, which is involved in embryogenesis and nervous system
349 development. This is one possible mechanism, and it remains speculative. More work needs to be done to
350 link the differences in genomic contact to differences in gene expression and ultimately to ASD.

351

352

353 **Discussion**

354

355 Here, we assess the impact of ASD-associated structural variants on genome organization and introduce a
356 pipeline for prioritizing variants that may contribute to the disorder by disrupting distal regulatory
357 interactions. We enhance the SuPreMo-Akita pipeline with two new features to evaluate the effects of
358 variants on specific nearby regions of interest. This software tool and our proof-of-principle analyses will
359 enable variant prioritization for other cohorts and biological contexts. Our analyses of ASD probands and
360 their unaffected siblings support a modest but consistent, hypothesis-generating signal that a subset of
361 ASD dnSVs preferentially disrupt regulatory chromatin interactions, particularly those involving
362 promoters of neuronal genes. Notably, we identified several candidate ASD de novo deletions predicted
363 to affect genome folding near risk genes. We validated one of our predictions using CRISPR genome
364 editing and iPSC-derived ExN cells, demonstrating that a 23 kb deletion overlapping a CTCF binding site
365 increases contacts between previously insulated genomic regions. This deletion results in misregulation of
366 neurodevelopmental genes across the genome and may be implicated in the proband's diagnosis, although
367 further studies are needed to confirm this; a patient variant causing changes in chromatin contacts, even
368 with accompanying gene expression changes, does not directly implicate the variant in ASD. We
369 examined publicly available neuronal Hi-C datasets and, while we found the general pattern at the

370 prioritized loci to match the Akita predictions, the resolution was insufficient for quantitative comparison.
371 Other high-scoring dnSVs remain to be tested experimentally.

372

373 Finding appropriate controls for structural variants—such as random length-matched SVs or ones from
374 healthy individuals—is challenging due to their likelihood of falling in protected regions or being generally
375 smaller. Studying variants in simplex families is especially valuable because the unaffected siblings share
376 the same genetic background as the proband, enhancing the relevance of our comparisons. However,
377 siblings are still more likely to possess damaging variants compared to unrelated individuals, reflecting
378 the genetic complexity of ASD and the challenges in diagnosis. Indeed, we found examples of sibling
379 dnSVs that are predicted to disrupt contacts of neuronal genes, even though they may not be causal for
380 ASD. Consequently, we did not expect drastic differences in variant effects between probands and
381 siblings, nor did we expect disruptive dnSVs to be present in all probands. Despite these challenges, the
382 ability to detect significant differences in disruption scores is encouraging and underscores the robustness
383 of our findings. This is the first evidence at a cohort scale that disrupted genome folding may play a role
384 in ASD.

385

386 Studying large structural variants poses significant challenges. Large variants are likely to contain many
387 potentially causal elements (genes, enhancers, chromatin boundaries) that are difficult to disentangle
388 computationally. Furthermore, results may be less reliable for dnSVs with low-confidence calls,
389 potentially impacting the statistical power of our cohort-wide analyses. When it comes to experimental
390 modeling, recapitulating large heterozygous variants, such as the 23 kb deletion on Chromosome 10, is
391 constrained by factors like PAM site availability, gRNA efficiency, and allelic differences. The WTC11
392 cell line lacks sufficient heterozygous SNPs for allele-specific Hi-C analysis that would mirror Akita's
393 allele agnostic predictions. To address these issues, we introduced a homozygous deletion. Although this
394 approach does not directly model the heterozygous patient and may overestimate gene expression
395 changes, it is a practical way to effectively isolate and confirm the impact of the deletion on genomic

396 contacts. Due to gRNA efficiency limitations, the CRISPR-induced deletion results in an early stop codon
397 that disrupts transcript continuity, differing from the in-frame deletion present in the proband. Despite
398 these limitations, the generated clonal cell line closely models the variant's effects in neurons. Because
399 *USP54* is not a known ASD or neurodevelopmental gene, and it is not functionally associated with the
400 DEGs we detected, we hypothesize that *USP54* is a bystander gene and that the DEGs result from
401 downregulation of *DDIT4* and/or other neuronal genes affected by the dnSV. Though, we cannot
402 disentangle contributions from altered 3D folding, loss of CTCF insulation, disruption of unmarked
403 regulatory elements, or changes to *USP54* transcript structure, all of which may contribute to the observed
404 effects. Furthermore, because our experimental system uses homozygous deletions, the magnitude of
405 expression changes may overestimate the effects of the heterozygous proband variant. Future work
406 focused on engineering a more precise heterozygous deletion could provide further insights into gene
407 expression changes and help identify potential functional phenotypes.

408
409 This work introduces a pipeline for prioritizing candidate disease variants and generating testable
410 hypotheses regarding their functional impact. Its application to ASD demonstrates that variant-induced
411 alterations in genome folding may contribute to the disorder and identifies a candidate causal deletion.
412 Ultimately, teasing apart ASD's complex etiology will require a holistic understanding of variant effects.
413 This may include new genetic underpinnings, which our study aims to predict with ML. Our study aims to
414 clarify the genetic underpinnings of such disorders by individually characterizing variant effects with the
415 SuPreMo-Akita workflow. Our updated software enables this strategy to be efficiently applied to other
416 genetic diseases and biological contexts to generate and prioritize testable hypotheses about potentially
417 causal variants.

418 Future work could enhance SuPreMo's utility by integrating it with other predictive models and
419 annotating variants based on their impact on epigenetic modifications and gene expression. Developing
420 models with better cell type specificity than Akita is a priority, because disease variants are expected to
421 have tissue-specific effects. Publicly available neuronal Hi-C datasets were examined but were too low-

422 resolution for quantitative analysis. We mitigated this limitation by utilizing publicly available ExN
423 PLAC-seq and ChIP-seq data to prioritize ASD variants and interpret Akita predictions, followed by
424 validations in ExNs. Following a similar strategy, the current pipeline can immediately be applied to non-
425 neuronal cell types and other disorders. Looking ahead, a cell type specific Akita model and other future
426 refinements to the SuPreMo ISM pipeline would further enhance our ability to uncover new disease-
427 associated variants for experimental validation. Because our experimental validation is currently limited
428 to a single locus, the generalizability of SuPreMo-Akita predictions in ASD remains to be established and
429 will require testing of additional loci. As experimental validation approaches become more precise and
430 high-throughput, it will be possible to test large numbers of SuPreMo predictions and utilize the results to
431 iteratively improve sequence-based variant prediction models like Akita. We envision an increased yield
432 of genome editing studies enabled by ML models that prioritize variants amongst the huge number that
433 could be tested, advancing our understanding of the molecular mechanisms underlying a wide array of
434 genetic disorders.

435

436

437 **Materials and Methods**

438

439 **Previously published data sources**

440 SFARI SSC proband and sibling dnSVs were previously called from short-read whole genome
441 sequencing data using the GATK-SV pipeline(Belyeu et al. 2021; Collins et al. 2021). PLAC-seq data is
442 from primary human mid-gestational ExNs(Song et al. 2020). ExN epigenetic data was downloaded from
443 publicly available sources. ChIP-seq data is from ENCODE with the following dataset IDs:
444 ENCSR489QDF for CTCF, ENCSR201NXX for H3K27me3, ENCSR818PER for H3K27ac, and
445 ENCSR411ZUA for H3K27me3. Neural progenitor cell (NPC) Hi-C data was previously
446 published(Keough et al. 2023). ASD genes are cataloged from three different datasets: SFARI
447 genes(Banerjee-Basu and Packer 2010), risk genes from an exome sequencing study(Satterstrom et al.

448 2020), and genes found from de novo risk scores(An et al. 2018). Gene exon coordinates used are from
449 GENCODE v46(Frankish et al. 2019).

450

451 **Akita model**

452 Akita(Fudenberg et al. 2020) is a convolutional neural network model that predicts the chromatin
453 interaction map for an input DNA sequence using no other information. The model was trained using
454 deeply-sequenced experimental Hi-C and Micro-C data from five cell lines (HFF, H1hESC, GM12878,
455 IMR-90, HCT116), processed at 2,048 bp resolution into pairwise contact frequency maps using *cooltools*
456 (Open 2C et al. 2024) (log observed/expected contact frequencies for all pairs of 2,048 bp bins). The input
457 to Akita is ~1 Mb (2^{20} bp) of 1-hot encoded DNA sequence. The model converts the sequence into a one-
458 dimensional embedding, which is then transformed into a two-dimensional ~1 Mb x ~1 Mb contact map
459 prediction at 2,048 bp resolution. Akita was trained to minimize the mean squared error (MSE) between
460 experimental and predicted contact maps, achieving a genome-wide average MSE of 0.14 on held-out test
461 set sequences (Pearson's $R = 0.61$, Spearman's $R = 0.56$). Performance across cell types depended
462 slightly on sequencing depth of the experimental maps, with Human Foreskin Fibroblast (HFF) cells
463 being the best predicted. Only limited differences were detected between predictions for different cell
464 types. This mirrors experimental maps, which are also largely similar across cell types, although further
465 model optimization could potentially improve cell type specificity on those genomic loci that do show
466 cell type differences in their chromatin interactions (see Discussion). Since none of the training cell types
467 was a neuronal cell type, we opted to use predictions for HFF. As described below, we used ExN PLAC-
468 seq and ChIP-seq data to further focus variant prioritization on effects in the developing brain.

469

470 **Variant scoring with SuPreMo-Akita**

471 To measure the predicted disruption on nearby chromatin contacts across 869 SVs, SuPreMo-Akita was
472 used. For each SV, this pipeline takes the 1 Mb reference sequence surrounding the variant (center
473 coordinate) and generates a 1 Mb mutated sequence with the alternate allele of the variant changed at the

474 appropriate location. Both sequences are input to the Akita model and the resulting contact frequency
475 maps are padded and masked so that each 2,048 bp bin from either map corresponds to a similar
476 sequence. The remaining regions of the maps—those outside of the SV itself—are then compared using
477 correlation and mean squared error (MSE). To get augmented scores, scores from four sequences were
478 averaged: 1) no augmentation, 2) 1 bp right shift, 3) 1 bp left shift, and 4) the reverse complement. Of
479 note, differences in scores across variant types could be partially due to how SuPreMo-Akita scores
480 different variant types, for instance duplications are treated like insertions of the duplicated sequence at its
481 5' end(Gjoni and Pollard 2024).

482

483 **Variant exclusions**

484 Only a subset of dnSVs were scored—they have to be above the length threshold, have known alternate
485 allele sequences (deletions, inversions, duplications, and complex variants), and be in regions where the
486 reference sequence is known. Scores represent changes in the region surrounding each variant, excluding
487 the variant itself. As a result, the size of these regions varies depending on the size of the variant. This
488 could overestimate the impact of very large variants, so we did not evaluate 73 variants larger than 700
489 kb. These variants could be tested with genome folding prediction models that use larger input sequences,
490 such as ORCA(Zhou 2022), however the resulting predictions would be at much lower resolution and
491 would preclude analysis of individual CREInts. Variants for which the alternate allele sequence is not
492 known were excluded from the analyses, because Akita needs the exact sequence to generate a prediction.
493 This includes insertions (SV types: *Alu*, LINE1, SVA, and INS) and translocations (SV type: CTX).
494 SuPreMo filters out variants that are greater in length than $\frac{2}{3}$ of the input sequence. Additionally, certain
495 variants do not get a score because the region that they are in has a composition of unknown sequence of
496 greater than 5%. Since CPX variants are not compatible with SuPreMo, we wrote custom code to generate
497 mutated sequences with those variants. However, these variant types are excluded from the CREInt-
498 weighted analyses (**Fig. 2, Supplemental Fig. S2**), since those analyses require using the SuPreMo
499 pipeline. In total, we generated scores for 598 dnSVs.

500 **Neuronal cis regulatory element interactions**

501 To annotate CREints, paired peak regions from primary human ExN PLAC-seq data were used (Song et
502 al. 2020). Here, we refer to each pair of regions as a loop and each single region as a loop anchor. Loops
503 were processed by grouping and filtering to generate regions of interest (ROIs) for weighted scoring
504 (**Supplemental Fig. S2A**). Only interchromosomal loops with anchors closer than 900 kb were
505 considered, as limited by Akita, which outputs contact frequency maps corresponding to a 917,504 bp
506 region. Then loops within 10 kb of each other were considered redundant and grouped together to result
507 in less pairs and better fit the Akita 2,048 bp bin resolution. For all the pairs with the last left anchor, the
508 right anchors that were within 10 kb were combined so that the new right anchor for all the pairs is the
509 same and includes all the previous right anchors. The same process was done on the left anchors of pairs
510 with the same right anchor. While all of these steps are also a part of how SuPreMo processes inputted
511 regions of interest for weighting, in this study we also took additional filtering steps. We only kept
512 CREints at least one anchor of which overlaps the promoter—defined as the 2 kb outside of the TSS—of
513 genes expressed in ExNs (Song et al. 2020). Lastly, after pairing CREints with variants, we only kept ones
514 where both loops of the CREint and the variant are less than 900 kb and therefore fit in the prediction
515 window. Note that any plotted CREints are not subject to this filtering but rather the initial PLAC-seq
516 pairs. While CREints may include non-regulatory contacts and introduce false positives (FP), the FP rate
517 will be consistent between probands and siblings, allowing for their fair comparison.

518

519 To calculate enrichment of dnSVs near CREints, the genome was split into 1 Mb bins and each bin was
520 annotated for whether it overlapped with a dnSV and a CREint region. A chi-squared test was used to
521 calculate the p -value.

522

523 **CREint weighted scoring**

524 For weighting scores at ROIs, contact frequency maps were generated as described above. Instead of
525 comparing the whole map, disruption tracks were generated by comparing each 1-bin-wide column in the

526 map and getting a list of 448 scores across all bins. Then a weight track was generated, which has a scalar
527 value in bins that overlap ROI and 1 in the rest of the bins. The mean of the disruption track is the
528 unweighted score and the mean of the disruption track multiplied times the weight track is the weighted
529 score. The weight track is generated by upscaling any bin that overlaps any ROI. ROIs can be given in the
530 form of a BED file for a custom set of regions, such as accessible regions from ATAC-seq, a paired BED
531 file, such as promoter contacts from PLAC-seq, or by just specifying ‘genes’ which will use a 2 kb region
532 centered at the TSS of every gene.

533

534 To find variants near CREints, CREints and variants were paired together if both CREint anchors and the
535 variant were all within 900 kb. Pairs where the variant overlapped either CREint anchor were removed. The
536 resulting 3,677 pairs were made up of 347 dnSVs and 2916 CREints. Disruption scores for this subset of
537 dnSVs were extracted from the existing set of scores. Then, for each pair, a shift for the prediction
538 window was calculated that would result in the pair being centered in the Akita input sequence. These
539 shifted windows were scored using SuPreMo and 10-fold up-weighting either all CREint anchors in the
540 window or only anchors of the paired CREint. This resulted in a score for each dnSV-CREint pair which
541 was summarized into one score per dnSV by taking the maximum across all CREint pairs.

542

543 **Criteria for variant prioritization**

544 We used the following criteria for prioritizing candidate dnSVs.

545 Required:

- 546 1. **Not on ASD gene:** Variant does not overlap ASD gene exon.
- 547 2. **No causal dnSV:** Proband does not have dnSV overlapping ASD gene exon.
- 548 3. **Good prediction:** Predicted maps for the reference genome around dnSV are similar to NPC
549 experimental Hi-C maps. This includes dnSVs for which the mean squared error (MSE) between
550 the Akita predicted and the experimental contact maps is less than the 85th percentile of MSE
551 across all scored variants.

- 552 4. **No sibling dnSV:** There are no similar variants in siblings. This includes proband dnSVs that
553 don't overlap by more than half of the variant region with more than half of any sibling dnSV
554 region.
- 555 5. **Disrupts CREint:** Variant results in changed contact at CREints. This includes dnSVs with
556 weighted disruption scores at CREints (**Fig. 2Biv**) larger than the 65th percentile across all
557 standard scores (**Fig. 1B**).
- 558 6. **Near ASD gene:** Variant is within 500 kb of an ASD gene.
- 559 7. **Disruptive:** Variant is disruptive to 3D genome folding of surrounding regions. This includes
560 dnSVs with disruption scores above the 65th percentile across all scores.

561 Optional:

- 562 8. **Not on expressed gene:** Variant does not overlap expressed gene (TPM > 0.5) exon.
- 563 9. **Not on ExN RE:** Variant does not overlap ExN regulatory elements, namely active enhancers
564 (H3K27ac), poised enhancers (H3K4me1), and poised promoters (H3K27me3) as defined by
565 their respective ChIP-seq peaks.
- 566 10. **Change on CREint:** Variant disruption focused on CREints, meaning weighted score (**Fig.**
567 **2Biii**) is higher than unweighted score (**Fig. 2Bii**).
- 568 11. **On CTCF:** Variant overlaps less than half of any ExN CTCF ChIP-seq peak.
- 569 12. **Deletion:** Variant is a deletion. These are the most straightforward to edit in cells.

570

571 Variants that passed all 7 required criteria were qualitatively evaluated. The selected three deletions
572 (**Supplemental Fig. S3**) were predicted to cause structural changes to the chromatin structure, as opposed
573 to just changes in contrast. The changed contacts align with nearby ASD genes and excitatory neuron
574 PLAC-seq loops correspond well with Akita-predicted contacts. Additionally, the deletion that was
575 selected for experiments had the most reproducible effect when augmenting maps with sequence shifting
576 and reverse complement.

577 CRISPR-engineered cell lines

578 The isogenic clonal iPSC lines were made by CRISPR-Cas9 system-mediated deletion. The WTC11 i³N
579 iPSC line with doxycycline-inducible Ngn2 integrated at the AAVS1 safe harbor locus was used as the
580 parental line. We designed four sgRNAs using CHOPCHOP (<https://chopchop.cbu.uib.no/>) to delete the
581 genomic region overlapping with the ASD variant and a CTCF site within the ASD variant. The designed
582 sgRNAs (**Supplemental Table S2**) were in vitro transcribed using the Precision gRNA Synthesis Kit
583 (Invitrogen, A29377), and Cas9-NLS protein was ordered from QB3 MacroLab at the University of
584 California, Berkeley. We assembled the Cas9/sgRNA complex by incubating the in vitro transcribed
585 sgRNAs and Cas9-NLS protein at 20-25°C for 15 min and delivered the complex into WTC11 i³N iPSCs
586 using nucleofection (Lonza, VPH-5012). After nucleofection, the cells were seeded into Matrigel-coated
587 (Corning, 354277) wells for recovery. 3-4 days later, we sorted live cells into 96-well plates with one cell
588 per well using fluorescence-activated cell sorting (FACS) to generate clonal cell lines. About two weeks
589 later, the viable clones were expanded. Meanwhile, we extracted genomic DNA from each clone using
590 QuickExtract DNA Extraction Solution (Biosearch Technologies, QE09050) and checked the genotype of
591 each clone using PCR and Sanger sequencing. This resulted in 6 clonal cell lines included in this
592 manuscript: 2 WT, 2 full deletion, and 2 CTCF deletion, each a pair of biological replicates.

593

594 ExN differentiation

595 The WTC11 i³N iPSCs were cultured on Matrigel-coated (Corning, 354277) plates and maintained in
596 mTeSR Plus media (STEMCELL Technologies, 100-0276), and passaged with Accutase (STEMCELL
597 Technologies, 07920) and 10- μ M ROCK inhibitor Y-27632 (STEMCELL Technologies, 72302). The
598 cells were grown with 5% CO₂ at 37°C and verified mycoplasma-free using the MycoAlert Mycoplasma
599 Detection Kit (Lonza, LT07-218). We differentiated the iPSCs into ExNs by using a two-step
600 differentiation protocol. First, we cultured iPSCs on Matrigel-coated plates with pre-differentiation media
601 with doxycycline (2 μ g/mL; Sigma-Aldrich, D9891) for three days and changed the media daily. Three
602 days later, the pre-differentiated cells were dissociated with Accutase (STEMCELL Technologies, 07920)

603 and subplated on Poly-L-Ornithine-coated (15 $\mu\text{g}/\text{mL}$; Sigma-Aldrich, P3655) plates with maturation
604 media with doxycycline. Then, the maturation media was changed seven days later by removing half of
605 the media from each well and adding the same amount of fresh media without doxycycline. The
606 differentiated neurons were collected two weeks after differentiation for experiments. The detailed
607 protocol is accessible at the ENCODE portal ([https://www.encodeproject.org/documents/d74fb151-366c-
608 4450-9fa0-31cc614035f9/](https://www.encodeproject.org/documents/d74fb151-366c-4450-9fa0-31cc614035f9/)).

609

610 **Hi-C**

611 Hi-C libraries were generated using the Arima-HiC+ kit (P/N A101020) according to the manufacturer's
612 protocol. Briefly, differentiated ExNs were fixed in culture plates with 2% PFA (Fisher Scientific F79-
613 500) at room temperature for 10 min. About 0.5 million cells were used as input for each Hi-C library.
614 The crosslinked chromatin DNA was treated with restriction digestion, biotinylation, proximal ligation.
615 The proximally ligated chromatin was sheared with a Covaris S220 sonicator to fragments between 300
616 and 1,000 bp. The shared chromatin was then indexed with the Accel-NGS 2S Plus DNA Library Kit
617 (Swift Biosciences, 21024) and amplified with KAPA Library Amplification Kit (Roche, KK2620). The
618 final libraries were purified with AMPure XP beads (Beckman Coulter, A63881) and sequenced on
619 NovaSeq with paired-end 100 bp sequencing.

620

621 For analyzing Hi-C data, the 4DN processing pipeline was used, as outlined here:

622 https://data.4dnucleome.org/resources/data-analysis/hi_c-processing-pipeline. In short, reads were
623 mapped to GRCh38 using BWA v0.7.18(Li and Durbin 2009). Valid Hi-C alignments were filtered using
624 pairtools v1.0.3(Open2C et al. 2024) and returned to a pairs file. Next, biological replicates were merged
625 using <https://github.com/4dn-dcic/docker-4dn-hic/blob/master/scripts/run-merge-pairs.sh>. Lastly, the
626 pairs files were converted to cool files using cooler v0.9.3(Abdennur and Mirny 2020). Plotted maps from
627 experimental Hi-C data are at a resolution of 1,000 bp. Each biological replicate was also processed
628 separately and the replicates were visually compared at the variant locus and found to be highly similar.

629 For contact frequency map visualization, cool files were preprocessed the same as the training datasets for
630 the Akita model(Krietenstein et al. 2020; Fudenberg et al. 2020) to allow for easy visual comparison.
631 Namely, Hi-C data was normalized with genome-wide iterative correction (ICE)(Imakaev et al. 2012).
632 Then, using *cooltools* v0.7.1, the matrices were smoothed using adaptive coarsegraining, normalized for
633 distance-dependent contact decay. The values were log scaled and limited to (-2,2). Then, again using
634 *cooltools* v0.7.1, they were linearly interpolated to fill missing values. Lastly, the maps were smoothed
635 using *astropy* v5.2.2 (Astropy Collaboration et al. 2022) convolution with a 2D Gaussian filter.

636

637 **RNA-seq**

638 RNA was extracted from two-week-old ExNs differentiated from iPSCs using the RNeasy Mini Kit
639 (Qiagen, 74104). Approximately 4 mg of extracted total RNA was used to prepare libraries for
640 sequencing using the TruSeq Stranded mRNA Library Prep Kit (Illumina, 20020594). Libraries were
641 sequenced on NextSeq 2000 with paired-end 100 bp sequencing.

642

643 RNA-seq libraries, comprising 6 samples were sequenced to an average depth of $8e7$ reads per sample.
644 RNA-seq reads were aligned to GRCh38.112 using STAR v2.7.11b in gene annotation mode(Dobin et al.
645 2013). Alignment, RNA-seq, and Insert Size quality control metrics were generated using Picard v3.1.1.
646 Sample quality was assessed using FastQC v0.12.1([CSL STYLE ERROR: reference with no printed
647 form.]) and MultiQC v1.22.2(Ewels et al. 2016).

648

649 Genes with more than 2 counts per million (cpm) in at least 2 of the 6 samples were retained for
650 differential gene expression analysis. Filtered genes were tested for differential expression with DESeq2
651 v1.44.0(Love et al. 2014) and considered significantly differentially expressed with an adjusted p -value <
652 0.05.

653

654 A Gene Ontology (GO)(Carlson 2019) over-representation analysis was performed to test if DEGs from
655 the full deletion are enriched in Biological Process (BP) terms compared to all expressed genes (R
656 package clusterProfiler(Wu et al. 2021) v4.8.3 and GO.db v3.18.0). Enriched terms were defined by a
657 Benjamini-Hochberg corrected p -value < 0.05 and > 30 DEGs in the category (**Supplemental Table S4**).
658 A weighted gene co-expression network analysis (WGCNA v1.73) was performed to identify gene
659 modules associated with full deletion status on 6 samples (2 WT, 2 CTCF deletion, and 2 full deletion
660 samples). Normalized counts from all six samples were used to construct an adjacency matrix (softPower
661 = 6, selected by scale-free topology fit). Using the topological overlap distance matrix, genes were
662 clustered into modules using dynamic tree cutting (deepSplit = 2, minClusterSize = 50) and merged by
663 eigengene similarity—resulting in 43 modules. Deletion status was encoded as a binary variable and
664 correlated with module eigengenes and gene expression using Pearson’s correlation with Student’s p -
665 values. Four modules were significantly associated with the deletion, three of which contained DDIT4.
666 GO enrichment analysis was performed for each module using the method described above. Due to the
667 low sample size potentially causing modules to be unstable, these modules should be viewed as
668 hypothesis-generating rather than definitive network structures.

669

670 **Code Availability**

671 SuPreMo V2 code is available as a Supplemental file and on GitHub at
672 <https://github.com/ketringjoni/SuPreMo/>.

673

674 **Data Access**

675

676 All raw and processed sequencing data generated in this study have been submitted to the NCBI Gene
677 Expression Omnibus (GEO; <https://www.ncbi.nlm.nih.gov/geo/>) under accession numbers GSE281283 and
678 GSE281327 for Hi-C and RNA-seq, respectively.

679

680 **Competing Interest Statement**

681

682 The authors declare no competing interest.

683

684

685 **Acknowledgements**

686

687 We thank Ian Jones for guidance with PLAC-seq data analysis interpretation. We thank Shuzhen Kuang
688 for input on Hi-C data analysis. We thank Jingjing Li for mentorship and feedback on the project. This
689 project was funded by NIH (grant #U01HL157989) and the Simons Foundation (grant #SFI-AN-AR-Data
690 Analysis-00019589).

691

692

693 **Author Contributions**

694

695 K.G. helped conceive the project, performed most computational analyses, and prepared the manuscript
696 and figures. X.R. performed all wet-lab experiments including CRISPR-Cas9 editing, cell
697 differentiations, and sample preparation for Hi-C and RNA-seq. A.E. performed RNA-seq, differential
698 expression, GO enrichment, and WGCNA analyses. Y.S. helped guide the project and managed the
699 experiments. K.S.P. conceived and managed the project and edited the manuscript. All authors reviewed
700 the manuscript.

701 **References**

- 702 Abdennur N, Mirny LA. 2020. Cooler: scalable storage for Hi-C data and other genomically labeled
703 arrays. *Bioinformatics* **36**: 311–316.
- 704 An J-Y, Lin K, Zhu L, Werling DM, Dong S, Brand H, Wang HZ, Zhao X, Schwartz GB, Collins RL, et
705 al. 2018. Genome-wide de novo risk score implicates promoter variation in autism spectrum
706 disorder. *Science* **362**. <http://dx.doi.org/10.1126/science.aat6576>.
- 707 The Astropy Collaboration, Price-Whelan AM, Lim PL, Earl N, Starkman N, Bradley L, Shupe
708 DL, Patil AA, Corrales L, Brasseur CE, et al. 2022. The Astropy Project: Sustaining and
709 Growing a Community-oriented Open-source Project and the Latest Major Release (v5.0) of the
710 Core Package.
<https://doi.org/10.48550/arXiv.2206.14220>
- 711
- 712 Banerjee-Basu S, Packer A. 2010. SFARI Gene: an evolving database for the autism research community.
713 *Dis Model Mech* **3**: 133–135.
- 714 Belyeu JR, Brand H, Wang H, Zhao X, Pedersen BS, Feusier J, Gupta M, Nicholas TJ, Brown J, Baird L,
715 et al. 2021. De novo structural mutation rates and gamete-of-origin biases revealed through genome
716 sequencing of 2,396 families. *Am J Hum Genet* **108**: 597–607.
- 717 Carlson M. 2019. *GO.db: A set of annotation maps describing the entire Gene Ontology*.
- 718 Chaste P, Leboyer M. 2012. Autism risk factors: genes, environment, and gene-environment interactions.
719 *Dialogues Clin Neurosci* **14**: 281–292.
- 720 Collins RL, Brand H, Karczewski KJ, Zhao X, Alföldi J, Francioli LC, Khera AV, Lowther C, Gauthier
721 LD, Wang H, et al. 2021. Author Correction: A structural variation reference for medical and
722 population genetics. *Nature* **590**: E55.
- 723 Dobin A, Davis CA, Schlesinger F, Drenkow J, Zaleski C, Jha S, Batut P, Chaisson M, Gingeras TR.
724 2013. STAR: ultrafast universal RNA-seq aligner. *Bioinformatics* **29**: 15–21.
- 725 Ewels P, Magnusson M, Lundin S, Käller M. 2016. MultiQC: summarize analysis results for multiple
726 tools and samples in a single report. *Bioinformatics* **32**: 3047–3048.
- 727 Fischbach GD, Lord C. 2010. The Simons Simplex Collection: a resource for identification of autism
728 genetic risk factors. *Neuron* **68**: 192–195.
- 729 Frankish A, Diekhans M, Ferreira A-M, Johnson R, Jungreis I, Loveland J, Mudge JM, Sisu C, Wright J,
730 Armstrong J, et al. 2019. GENCODE reference annotation for the human and mouse genomes.
731 *Nucleic Acids Res* **47**: D766–D773.
- 732 Fudenberg G, Kelley DR, Pollard KS. 2020. Predicting 3D genome folding from DNA sequence with
733 Akita. *Nat Methods* **17**: 1111–1117.
- 734 Geschwind DH. 2011. Genetics of autism spectrum disorders. *Trends Cogn Sci* **15**: 409–416.
- 735 Gjoni K, Pollard KS. 2024. SuPreMo: a computational tool for streamlining in silico perturbation using

- 736 sequence-based predictive models. *Bioinformatics* **40**.
 737 <http://dx.doi.org/10.1093/bioinformatics/btae340>.
- 738 Grove J, Ripke S, Als TD, Mattheisen M, Walters RK, Won H, Pallesen J, Agerbo E, Andreassen OA,
 739 Anney R, et al. 2019. Identification of common genetic risk variants for autism spectrum disorder.
 740 *Nat Genet* **51**: 431–444.
- 741 Gunsalus LM, Keiser MJ, Pollard KS. 2023a. discovery of repetitive elements as key sequence
 742 determinants of 3D genome folding. *Cell Genom* **3**: 100410.
- 743 Gunsalus LM, McArthur E, Gjoni K, Kuang S, Pittman M, Capra JA, Pollard KS. 2023b. Comparing
 744 chromatin contact maps at scale: methods and insights. *Res Sq.* <http://dx.doi.org/10.21203/rs.3.rs-2842981/v1>.
 745
- 746 Huang W-H, Guenther CJ, Xu J, Nguyen T, Schwarz LA, Wilkinson AW, Gozani O, Chang HY,
 747 Shamloo M, Luo L. 2016. Molecular and neural functions of Rail, the causal gene for Smith-
 748 Magenis syndrome. *Neuron* **92**: 392–406.
- 749 Huguet G, Benabou M, Bourgeron T. 2016. The Genetics of Autism Spectrum Disorders. In *A Time for*
 750 *Metabolism and Hormones* (eds. P. Sassone-Corsi and Y. Christen), Springer, Cham (CH).
- 751 Imakaev M, Fudenberg G, McCord RP, Naumova N, Goloborodko A, Lajoie BR, Dekker J, Mirny LA.
 752 2012. Iterative correction of Hi-C data reveals hallmarks of chromosome organization. *Nat Methods*
 753 **9**: 999–1003.
- 754 Iossifov I, O’Roak BJ, Sanders SJ, Ronemus M, Krumm N, Levy D, Stessman HA, Witherspoon KT,
 755 Vives L, Patterson KE, et al. 2014. The contribution of de novo coding mutations to autism spectrum
 756 disorder. *Nature* **515**: 216–221.
- 757 Kelley DR. 2020. Cross-species regulatory sequence activity prediction. *PLoS Comput Biol* **16**:
 758 e1008050.
- 759 Keough KC, Whalen S, Inoue F, Przytycki PF, Fair T, Deng C, Steyert M, Ryu H, Lindblad-Toh K,
 760 Karlsson E, et al. 2023. Three-dimensional genome rewiring in loci with human accelerated regions.
 761 *Science* **380**: eabm1696.
- 762 Kraft K, Magg A, Heinrich V, Riemenschneider C, Schöpflin R, Markowski J, Ibrahim DM, Acuna-
 763 Hidalgo R, Despang A, Andrey G, et al. 2019. Serial genomic inversions induce tissue-specific
 764 architectural stripes, gene misexpression and congenital malformations. *Nat Cell Biol* **21**: 305–310.
- 765 Kragsteven BK, Spielmann M, Paliou C, Heinrich V, Schöpflin R, Esposito A, Annunziatella C, Bianco
 766 S, Chiariello AM, Jerković I, et al. 2018. Dynamic 3D chromatin architecture contributes to
 767 enhancer specificity and limb morphogenesis. *Nat Genet* **50**: 1463–1473.
- 768 Krietenstein N, Abraham S, Venev SV, Abdennur N, Gibcus J, Hsieh T-HS, Parsi KM, Yang L, Maehr R,
 769 Mirny LA, et al. 2020. Ultrastructural Details of Mammalian Chromosome Architecture. *Mol Cell*
 770 **78**: 554–565.e7.
- 771 Krumm A, Duan Z. 2019. Understanding the 3D genome: Emerging impacts on human disease. *Semin*
 772 *Cell Dev Biol* **90**: 62–77.
- 773 Kurth I, Klopfacki E, Stricker S, van Oosterwijk J, Vanek S, Altmann J, Santos HG, van Harssel JJT, de
 774 Ravel T, Wilkie AOM, et al. 2009. Duplications of noncoding elements 5’ of SOX9 are associated

- 775 with brachydactyly-anonychia. *Nat Genet* **41**: 862–863.
- 776 Laugsch M, Bartusel M, Rehim R, Alirzayeva H, Karaolidou A, Crispatsu G, Zentis P, Nikolic M,
777 Bleckwehl T, Kolovos P, et al. 2019. Modeling the Pathological Long-Range Regulatory Effects of
778 Human Structural Variation with Patient-Specific hiPSCs. *Cell Stem Cell* **24**: 736–752.e12.
- 779 Li H, Durbin R. 2009. Fast and accurate short read alignment with Burrows–Wheeler transform.
780 *Bioinformatics* **25**: 1754–1760.
- 781 Liu Z, Tan S, Zhou L, Chen L, Liu M, Wang W, Tang Y, Yang Q, Chi S, Jiang P, et al. 2023. SCGN
782 deficiency is a risk factor for autism spectrum disorder. *Signal Transduct Target Ther* **8**: 3.
- 783 Love MI, Huber W, Anders S. 2014. Moderated estimation of fold change and dispersion for RNA-seq
784 data with DESeq2. *Genome Biol* **15**: 550.
- 785 More RP, Warriar V, Brunel H, Buckingham C, Smith P, Allison C, Holt R, Bradshaw CR, Baron-Cohen
786 S. 2023. Identifying rare genetic variants in 21 highly multiplex autism families: the role of
787 diagnosis and autistic traits. *Mol Psychiatry* **28**: 2148–2157.
- 788 Nakamura T, Ueda J, Mizuno S, Honda K, Kazuno A-A, Yamamoto H, Hara T, Takata A. 2024.
789 Topologically associating domains define the impact of de novo promoter variants on autism
790 spectrum disorder risk. *Cell Genom* **4**: 100488.
- 791 Open2C, Abdennur N, Fudenberg G, Flyamer IM, Galitsyna AA, Goloborodko A, Imakaev M, Venev
792 SV. 2024. Pairtools: from sequencing data to chromosome contacts. *PLoS Comput Biol* **20**:
793 e1012164.
- 794 Rylaarsdam L, Guemez-Gamboa A. 2019. Genetic Causes and Modifiers of Autism Spectrum Disorder.
795 *Front Cell Neurosci* **13**: 385.
- 796 Satterstrom FK, Kosmicki JA, Wang J, Breen MS, De Rubeis S, An J-Y, Peng M, Collins R, Grove J,
797 Klei L, et al. 2020. Large-Scale Exome Sequencing Study Implicates Both Developmental and
798 Functional Changes in the Neurobiology of Autism. *Cell* **180**: 568–584.e23.
- 799 Short PJ, McRae JF, Gallone G, Sifrim A, Won H, Geschwind DH, Wright CF, Firth HV, FitzPatrick DR,
800 Barrett JC, et al. 2018. De novo mutations in regulatory elements in neurodevelopmental disorders.
801 *Nature* **555**: 611–616.
- 802 Sikic M. 2023. Facilitating genome structural variation analysis. *Nat Methods* **20**: 491–492.
- 803 Song M, Pebworth M-P, Yang X, Abnoui A, Fan C, Wen J, Rosen JD, Choudhary MNK, Cui X, Jones
804 IR, et al. 2020. Cell-type-specific 3D epigenomes in the developing human cortex. *Nature* **587**: 644–
805 649.
- 806 Sun JH, Zhou L, Emerson DJ, Phyto SA, Titus KR, Gong W, Gilgenast TG, Beagan JA, Davidson BL,
807 Tassone F, et al. 2018. Disease-Associated Short Tandem Repeats Co-localize with Chromatin
808 Domain Boundaries. *Cell* **175**: 224–238.e15.
- 809 Symmons O, Pan L, Remeseiro S, Aktas T, Klein F, Huber W, Spitz F. 2016. The Shh Topological
810 Domain Facilitates the Action of Remote Enhancers by Reducing the Effects of Genomic Distances.
811 *Dev Cell* **39**: 529–543.
- 812 van Bemmelen JG, Galupa R, Gard C, Servant N, Picard C, Davies J, Szempruch AJ, Zhan Y, Żylicz JJ,

- 813 Nora EP, et al. 2019. The bipartite TAD organization of the X-inactivation center ensures opposing
814 developmental regulation of Tsix and Xist. *Nat Genet* **51**: 1024–1034.
- 815 van Berkum NL, Lieberman-Aiden E, Williams L, Imakaev M, Gnirke A, Mirny LA, Dekker J, Lander
816 ES. 2010. Hi-C: a method to study the three-dimensional architecture of genomes. *J Vis Exp*.
817 <http://dx.doi.org/10.3791/1869>.
- 818 Wang C, Ward ME, Chen R, Liu K, Tracy TE, Chen X, Xie M, Sohn PD, Ludwig C, Meyer-Franke A, et
819 al. 2017. Scalable Production of iPSC-Derived Human Neurons to Identify Tau-Lowering
820 Compounds by High-Content Screening. *Stem Cell Reports* **9**: 1221–1233.
- 821 Weiner DJ, Wigdor EM, Ripke S, Walters RK, Kosmicki JA, Grove J, Samocha KE, Goldstein JI, Okbay
822 A, Bybjerg-Grauholm J, et al. 2017. Polygenic transmission disequilibrium confirms that common
823 and rare variation act additively to create risk for autism spectrum disorders. *Nat Genet* **49**: 978–985.
- 824 Weischenfeldt J, Ibrahim DM. 2023. When 3D genome changes cause disease: the impact of structural
825 variations in congenital disease and cancer. *Curr Opin Genet Dev* **80**: 102048.
- 826 Willsey HR, Willsey AJ, Wang B, State MW. 2022. Genomics, convergent neuroscience and progress in
827 understanding autism spectrum disorder. *Nat Rev Neurosci* **23**: 323–341.
- 828 Wu T, Hu E, Xu S, Chen M, Guo P, Dai Z, Feng T, Zhou L, Tang W, Zhan L, et al. 2021. clusterProfiler
829 4.0: A universal enrichment tool for interpreting omics data. *Innovation (Camb)* **2**: 100141.
- 830 Xia Q, Zheng H, Li Y, Xu W, Wu C, Xu J, Li S, Zhang L, Dong L. 2024. SMURF1 controls the
831 PPP3/calcineurin complex and TFEB at a regulatory node for lysosomal biogenesis. *Autophagy* **20**:
832 735–751.
- 833 Zagirova D, Kononkova A, Vaulin N, Khrameeva E. 2024. From compartments to loops: understanding
834 the unique chromatin organization in neuronal cells. *Epigenetics Chromatin* **17**: 18.
- 835 Zhou J. 2022. Sequence-based modeling of three-dimensional genome architecture from kilobase to
836 chromosome scale. *Nat Genet* **54**: 725–734.
- 837 Zhou J, Park CY, Theesfeld CL, Wong AK, Yuan Y, Scheckel C, Fak JJ, Funk J, Yao K, Tajima Y, et al.
838 2019. Whole-genome deep-learning analysis identifies contribution of noncoding mutations to
839 autism risk. *Nat Genet* **51**: 973–980.
- 840 Zhou J, Theesfeld CL, Yao K, Chen KM, Wong AK, Troyanskaya OG. 2018. Deep learning sequence-
841 based ab initio prediction of variant effects on expression and disease risk. *Nat Genet* **50**: 1171–
842 1179.
- 843 Babraham bioinformatics - FastQC A quality control tool for high throughput sequence data.
844 <http://www.bioinformatics.babraham.ac.uk/projects/fastqc/> (Accessed August 16, 2024a).
- 845 Open2C, Abdennur N, Abraham S, Fudenberg G, Flyamer IM, Galitsyna AA, Goloborodko A, Imakaev
846 M, Oksuz BA, Venev SV, et al. 2024. *Cooltools*: Enabling high-resolution Hi-C analysis in Python.
847 PLOS Computational Biology. *PLOS Computational Biology* **20**(5):e1012067.

848

849

850 **Figure 1. ASD dnSVs are predicted to be more disruptive to 3D genome folding than controls. A.**
851 SuPreMo-Akita workflow for scoring variant disruption to genome folding. Variant information is
852 inputted into SuPreMo-Akita, which in turn generates reference and alternate sequence pairs and inputs
853 those into Akita. It then processes the resulting maps and compares them to generate disruption scores. **B.**
854 Distribution of disruption scores for dnSVs from probands (pink) and siblings (blue). Mann-Whitney *U*
855 test *p*-value is 0.039 and Cohen's *d* is 0.18. **C.** Disruption scores plotted against dnSV length. *P*-value of
856 linear model predicting scores from length (red line) is shown. Dashed black lines are length cutoffs for
857 the four categories in Fig. 1 C-D. **D.** Disruption scores across variant length quantiles, Q1-Q4, for
858 proband and sibling dnSVs. Length quantile cutoffs are 147 bp, 3,976 bp, and 32,549 bp. Numbers of
859 dnSVs per quantile are as follows: 78 and 72 in Q1, 77 and 73 in Q2, 97 and 51 in Q3, and 97 and 53 in
860 Q4 for probands and siblings, respectively. **E.** Disruption scores across variant types—duplications (DUP),
861 deletions (DEL), complex variants (CPX), and inversions (INV)—including both proband and sibling
862 dnSVs. Tukey HSD FDR-corrected *p*-value between DUP and DEL is 8.3e-04. **F.** SV length across SV
863 types. Tukey HSD FDR-corrected *p*-value between DUP and DEL is 2.5e-07. **G.** Disruption scores across
864 length quantiles for probands (left) and sibling (right) dnSVs separated by whether the variant coordinates
865 overlap at least one CTCF binding site (purple) or not (gray) using ChIP-seq data from ExNs. Mann-
866 Whitney *U* test FDR-corrected *p*-value for Q4 is 0.006 and 0.630 for proband and sibling dnSVs,
867 respectively.
868

869 **Figure 2. Neuronal regulatory element interactions are indirectly disrupted by variants in ASD. A.**

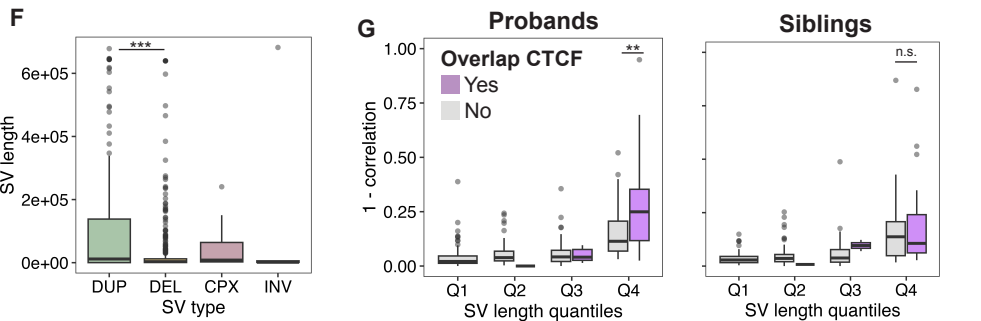
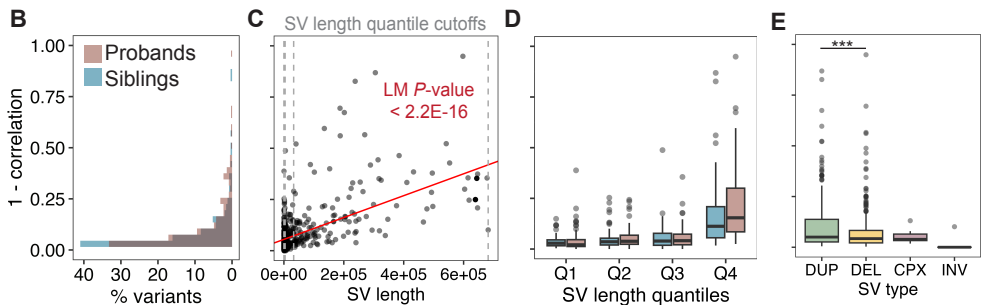
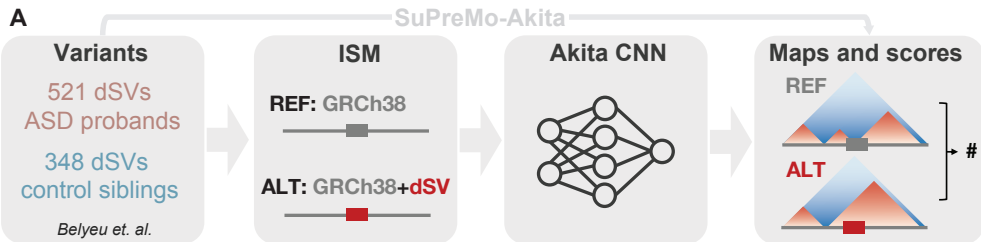
870 Schematic of SuPreMo-Akita implementation of weighted scoring. Unweighted score is the mean of the
871 disruption track (purple). For the weighted score, each value in the disruption track is multiplied by the
872 corresponding value of a weight track (orange, several options shown) before taking the average for the
873 window. The weight track may be generated from PLAC-seq paired regions, custom input regions, or
874 transcription start sites (TSSs). If PLAC-seq data is inputted, it will be processed to filter and condense
875 loops (**Methods, Supplemental Fig. S2A**). **B.** Disruption scores for a subset of dnSVs that are close
876 enough to CREints to both be in the same Akita prediction window. Scores, from top to bottom,
877 correspond to: (i) scores without weighting, (ii) scores where CREint anchors are upweighted 10-fold,
878 (iii) scores only comparing contacts involving CREint anchors. These distributions show that differences
879 between probands and siblings are greater with weighted scores that utilize CREints.

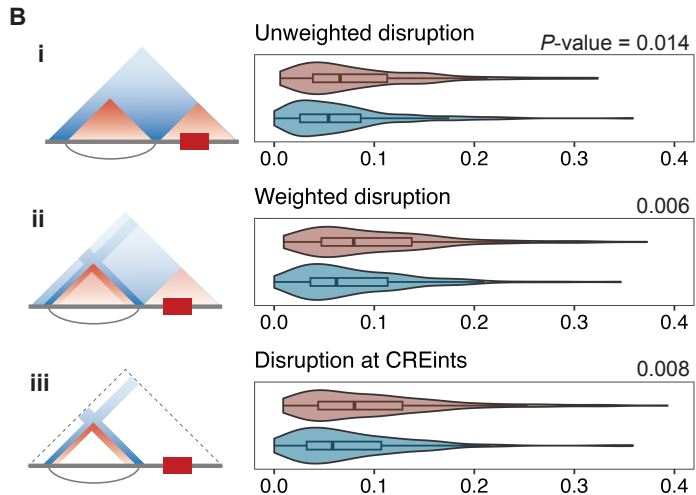
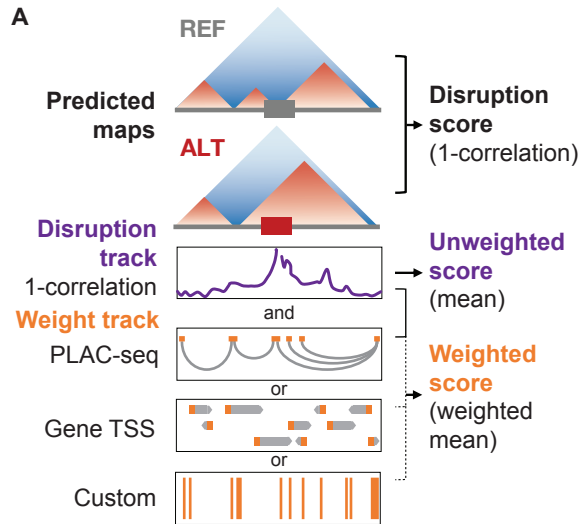
880

881 **Figure 3. Convolutional neural network correctly predicted effect of an ASD deletion on chromatin**

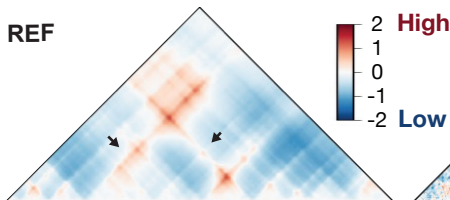
882 **contacts.** Predicted (left) and experimental (right) contact frequency maps for the reference genome (top),
883 reference genome with the 23 kb Chromosome 10 deletion (middle) and the difference between the two
884 (bottom). Genes in the corresponding ~917 kb region shown below maps. Arrows point to two regions
885 with changes in contact.

886

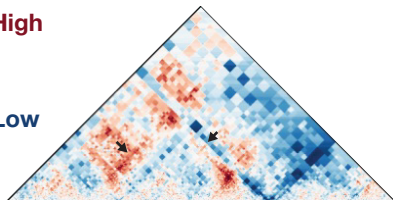




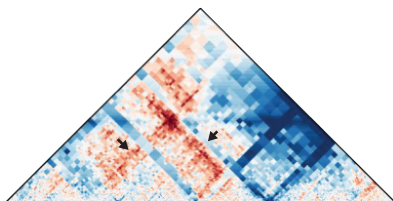
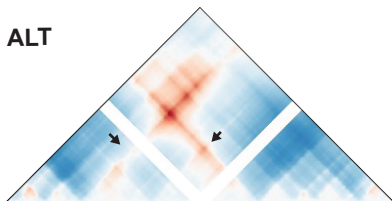
Akita predictions



Experimental HiC



ALT



REF-ALT

